

*First Experimental Campaign to
Demonstrate STARDUST-Upgrade Facility
Diagnostics Capability to Investigate LOVA
Conditions*

**L. A. Poggi, A. Malizia, J. F. Ciparisse,
M. Gelfusa, A. Murari, S. Pierdiluca,
E. Lo Re & P. Gaudio**

Journal of Fusion Energy

ISSN 0164-0313

J Fusion Energy

DOI 10.1007/s10894-015-9964-x



Your article is protected by copyright and all rights are held exclusively by Springer Science +Business Media New York. This e-offprint is for personal use only and shall not be self-archived in electronic repositories. If you wish to self-archive your article, please use the accepted manuscript version for posting on your own website. You may further deposit the accepted manuscript version in any repository, provided it is only made publicly available 12 months after official publication or later and provided acknowledgement is given to the original source of publication and a link is inserted to the published article on Springer's website. The link must be accompanied by the following text: "The final publication is available at link.springer.com".

First Experimental Campaign to Demonstrate STARDUST-Upgrade Facility Diagnostics Capability to Investigate LOVA Conditions

L. A. Poggi¹ · A. Malizia¹ · J. F. Ciparisse¹ · M. Gelfusa¹ · A. Murari² · S. Pierdiluca¹ · E. Lo Re¹ · P. Gaudio¹

© Springer Science+Business Media New York 2015

Abstract Given the urgent need to converge on precise guidelines for accident management in nuclear fusion plants, an experimental campaign has been carried out on the “STARDUST-Upgrade” facility for dust mobilization phenomena investigation at the University of Rome Tor Vergata. The main purpose of this preliminary work was to test the “STARDUST-Upgrade” facility capability to investigate Loss of Vacuum Accidents (LOVAs) and their thermo fluid-dynamic consequences. In fact, upper ports of “STARDUST-Upgrade” were used as inlet ports, reproducing coolant loss consequences from the upper part of the vacuum vessel in the International Thermonuclear Experimental Reactor (ITER). The facility was tested with the aim of reproducing LOVAs thermo fluid-dynamic consequences not only from lower and equatorial level of an ITER-like vacuum vessel but also from upper part of it. The diagnostics required for these experimental studies and the results of this first experimental campaign are presented.

Keywords Nuclear fusion safety · Dust mobilization · STARDUST-Upgrade · LOVA

Introduction

Fusion power is a promising long-term candidate to satisfy increasing global energy demand. Substantial fusion power has been produced in two large magnetic confinement devices: TFTR (10.7 MW, Princeton, NJ, USA) and JET (16 MW, Culham, United Kingdom). Moreover, construction for a 500 MW International Thermonuclear Experimental Reactor (ITER) has begun in Cadarache, France. ITER is intended to prove the viability of fusion as an energy source, and to collect the data necessary for the design and subsequent operation of the first electricity-producing fusion power plant. The ITER Agreement was signed by China, the European Union, India, Japan, Korea, Russia and the United States.

An important issue related to future nuclear fusion reactors is the large amounts of dust (aerosol particulate and flakes) produced by energetic plasma–surface interactions (Plasma-Material Interactions, PMIs) due to several mechanisms (plasma disruptions, edge localized modes ELM and vertical displacement events VDE) [1–4]. These mechanisms can cause significant erosion of vacuum vessel and divertor materials. A sizeable portion of the eroded material does not adhere to surfaces and dust is generated. Dust is capable of being re-suspended in case of events like LOVA (loss of vacuum accident) [5–8]. The dust size expected in nuclear fusion experiments (such as ITER) is in the order of microns (between 0.1 and 1000 μm) [5–9]. Re-suspension phenomena in case of LOVAs can cause serious hazard to the health of the operators (since particles are radioactive and of breathable size [10–12]) and can furthermore cause explosions compromising the integrity of the device and producing non-negligible hazard for the ambient [13]. Hence, nowadays the dust re-suspension due to LOVAs is one of the key factors for safety of workers

✉ L. A. Poggi
poggi@ing.uniroma2.it

¹ Associazione EUROFUSION-ENEA, Department of Industrial Engineering, University of Rome Tor Vergata, Via del Politecnico 1, 00133 Rome, Italy

² Consorzio RFX-Associazione EUROFUSION-ENEA per la Fusione, 35127 Padua, Italy

and security of nuclear plants in projects like ITER and DEMO (the foreseen Demonstration Power Plant).

Several experiments carried out by QEPM Research Group and other contributors demonstrated that the exchange flows of dust depend on number, position, length and shape of breaches, pressure and temperature conditions and type of fluid [14–31].

Given the urgent need to converge on precise guidelines for accident management in nuclear fusion plants, an experimental campaign on dust mobilization phenomena has been carried out at the University of Rome Tor Vergata since 2007, in the framework of the activities of the Quantum Electronics Plasma Physics and Materials (QEPM) Research Group. The QEPM Research Group developed a facility (“STARDUST”, Small Tank for Aerosol Removal and DUST) in order to reproduce the thermo fluid-dynamic conditions comparable to those expected inside the vacuum vessel of the next generation of experiments (such as ITER) in case of LOVAs due to small air leakage for two different positions of the leak, at the equatorial port level and at the divertor port level [18–34]. The dust used inside the “STARDUST” facility presented particle sizes and physical characteristics comparable with those created inside the vacuum vessel of nuclear fusion experiments, and it was made of tungsten, stainless steel and carbon, similarly to that produced inside the vacuum vessel of a fusion reactor (as predicted by the Generic Site Safety Report ITER-GSSR [35]). The consequences of dust re-suspension due to a LOVA event have been deeply analyzed by QEPM Research Group with “STARDUST” facility in previous experimental campaign in which the facility was demonstrated to be capable of reproducing thermo fluid-dynamic conditions and the dust resuspension fraction comparable to those expected inside the VV (Vacuum Vessel) of a nuclear fusion power plant such as ITER in case of LOVAs [18–31]. Using “STARDUST” facility QEPM Research Group developed and validated an extruded 2D thermo-fluid dynamic model [17, 24, 25, 30, 32] to analyze the effect of a LOVA on dust. Optical techniques (PIV [33], Shadowgraph [31, 34]) and numerical algorithms have been used to perform dust tracking during resuspension.

Given several limitation of “STARDUST” facility (it was not possible to simulate LOCAs; field of view inside the chamber was small for imaging needs; and it was not possible to replicate LOVAs for more than one accidental configuration [31, 33, 34]) the QEPM Research Group designed and implemented mechanical modifications to the facility.

After “STARDUST” facility was dismantled, an improved facility (“STARDUST-Upgrade”) to reproduce dust re-suspension phenomena was completed in

September 2014 and a preliminary work on this new facility had been carried out to test its capability to investigate LOVAs and their thermo fluid-dynamic consequences. The upper ports of “STARDUST-Upgrade” were used as air inlet ports, reproducing both LOVA and coolant loss consequences from the upper ports of the vacuum vessel in ITER. Pressurization experiments have been performed at two different air flow rates (27 and 40 l/min) to achieve several pressurization rates from about 250 to 400 Pa/s, so including rates expected in GSSR Report in case of a LOVA event [35]. Air flowed inside the facility’s vacuum chamber at room temperature from two different upper ports (C and D, see Figs. 2, 3), to simulate LOVAs consequences from the upper internal wall of an ITER-like vacuum vessel. A vacuum rupture in the upper part of the vessel could involve cooling fluids causing not only chamber pressurization and air intake but also refrigerant intake inside the vessel. However, for this first experimental campaign the facility was operated using air as a model fluid. In addition, for local air velocity calculation (in the point corresponding to the vessel part causing the vacuum rupture), pressure transducers array have been positioned inside “STARDUST-Upgrade” at the outlet of port C to measure differential pressure of the air flow during pressurization experiments simulating LOVAs consequences at different air flow rates and initial internal pressure of the chamber. Pressure transducers’ voltage output (mV) was acquired and converted into differential pressure (Pa) according to its sensitivity, and saved for air velocity calculation and error analysis.

In conclusion, in this preliminary work we wanted to measure local air velocity at 1 cm from inlet port used for air intake inside the facility and to measure temperature of the chamber and absolute pressure of the chamber. With “STARDUST-Upgrade” facility the vacuum rupture was reproducible not only from lower and mid-plane section but also from its upper section, corresponding respectively to lower, equatorial and upper section of an ITER-like vacuum vessel. This is just a first step of the experimental campaign carried out by QEPM Research Group, in terms of reproduction of the thermo fluid-dynamics comparable to that expected in vacuum rupture of nuclear fusion reactor vessel. As a preliminary work to characterize the environment in which the dust mobilization phenomena occur hence we performed a fine tuning of the facility with the aim to reach the scope of the experimental campaign.

The diagnostics required for these experimental studies, the procedures, and the results of this first experimental campaign are presented, including a comparison with predictions obtained with preliminary CFD (Computational Fluid Dynamics) model developed by QEPM Research Group.

STARDUST-Upgrade Facility Overview

“STARDUST-Upgrade” facility (Small Tank for Aerosol Removal and DUST—Upgrade) is composed of a cylindrical stainless steel vacuum chamber connected with diagnostics and data acquisition system that ensure thermo fluid-dynamic conditions comparable to that present in a fusion reactor vacuum vessel during LOVAs (e.g. that prescribed by the Generic Site Safety Report—GSSR [35]). The QEPM Research Group has designed and implemented mechanical modifications to “STARDUST” in order to get a facility with a bigger field of view through the introduction of new windows with a larger diameter together with the introduction of new air inlet and different lid configurations, as shown in Fig. 1 [36].

In its new configuration “STARDUST-Upgrade” facility was used to reproduce not only the consequences of a LOVA from the equatorial or divertor (i.e. lower) level but also from the new upper ports C and D shown in Figs. 2 and 3.

These implementation have been designed in 3D with the software SOLIDWORKS and the mechanical resistance has been tested numerically (with the same software) to verify the mechanical resistance of the new facility under the experimental boundary conditions expected to reproduce LOVAs [27]. The final layout of the facility has been design and built joining the best characteristics of the different layouts numerically tested [36]. Main dimensions of the facility are reported in Table 1.

Furthermore, a functional scheme of the facility is presented in Fig. 4. During every experiment data acquisition

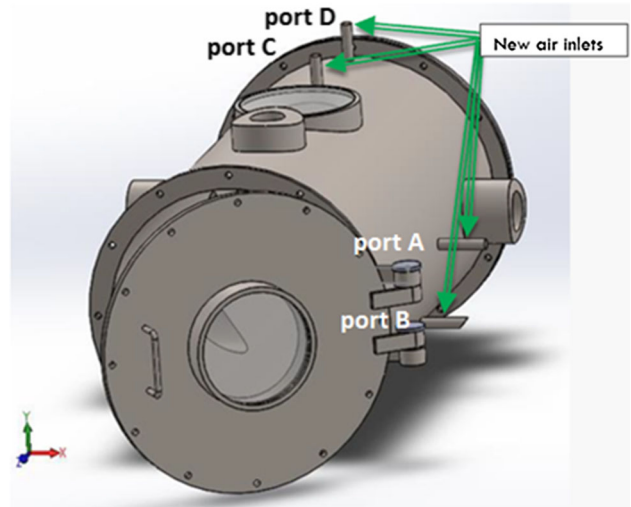


Fig. 2 New air inlet ports for “STARDUST-Upgrade” facility

was possible for the following quantities: thermocouples temperatures [T1 (°C), T2 (°C), T3 (°C), T4 (°C)], actual internal pressure [Ps (Pa)], inlet air flow rate (l/min), differential pressure $P\Delta$ from transducers array (Pa) and any other signal received by the universal cards of the acquisition system [4]. Voltage signal (mV) from the transducers array was converted into differential pressure (Pa) according to transducers sensitivity (XCE-093-2D High Temperature Miniature Pressure Transducers [37, 38]).

In order to correctly reproduce LOVAs similarly to those expected for ITER vacuum vessel for any sealing failure, thermo fluid-dynamic conditions were controlled by the system. Boundary conditions, in terms of initial

Fig. 1 New features in “STARDUST-Upgrade” experimental layout [36]

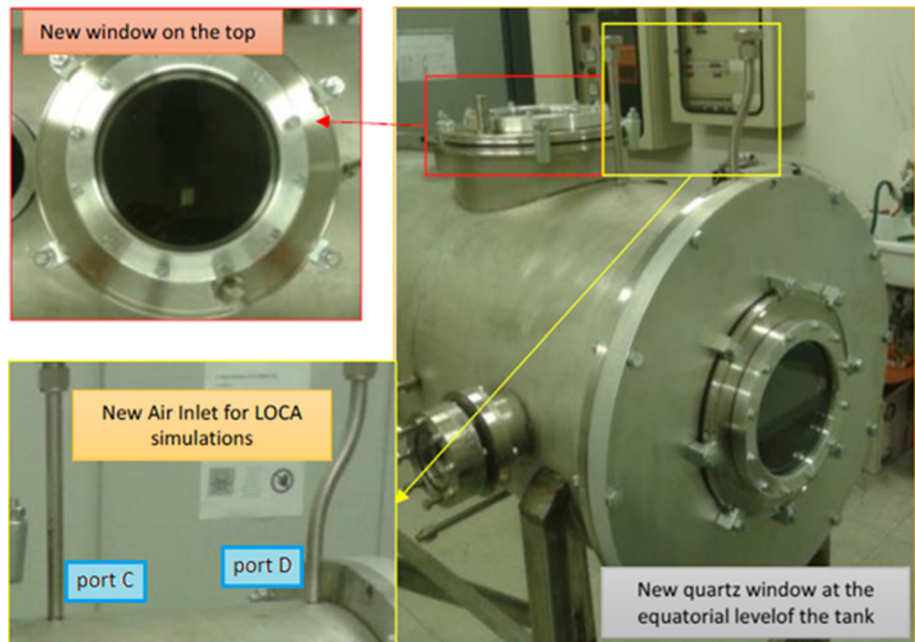


Fig. 3 “STARDUST” facility picture showing its ports corresponding to divertor equatorial and upper level of an ITER-like vacuum vessel

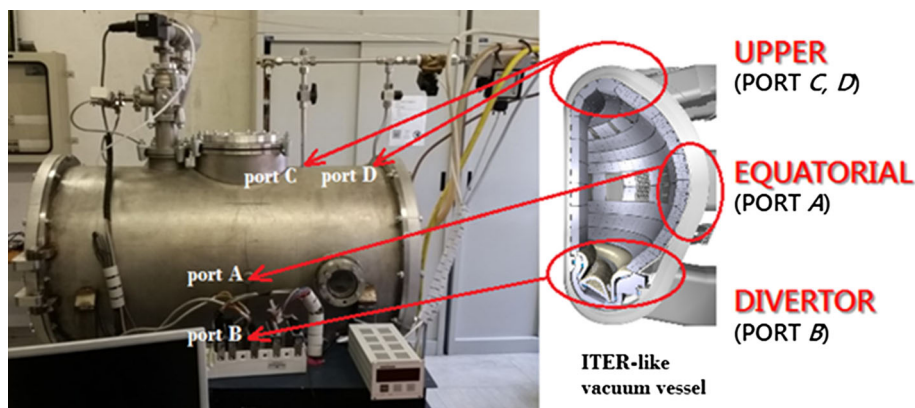


Table 1 Main dimensions of “STARDUST-Upgrade” facility [36]

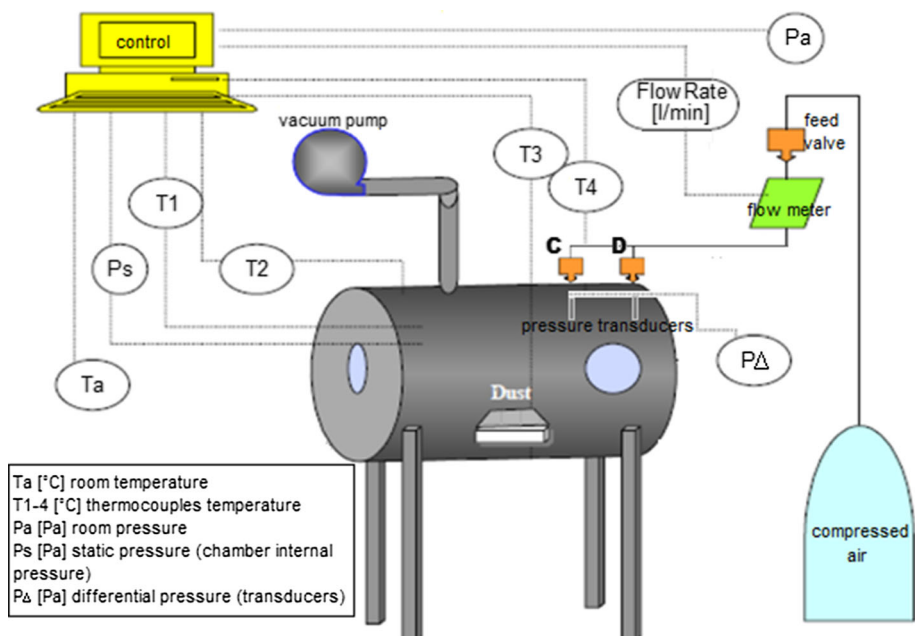
| | |
|---|------|
| Chamber external length [mm] | 920 |
| Chamber internal diameter [mm] | 490 |
| Lids external diameter [mm] | 570 |
| Lid thickness [mm] | 10 |
| Lid's windows diameter [mm] | 79 |
| Chamber internal volume [m ³] | 0.17 |

internal pressure of the vacuum chamber (i.e. “vacuum level”) and air flow rate entering the chamber, were achieved using a vacuum pump, and air compressed delivery system respectively, both remote controlled. Internal temperature was measured by four J-thermocouples placed inside the chamber. Internal pressure was measured by two gauges depending on the actual vacuum

level. Edwards pressure gauge (ASG-2000-NW16, Edwards, Crawley, UK) covered pressure range from 1000 to 2000 mbar. For higher vacuum levels (pressure below 1000 mbar) a Pirani gauge was used (Alcatel AP 1004 Pirani Gauge, Alcatel Vacuum Technology, Annecy, France [39]). Pirani gauge covered a pressure range from 0.0005 to 1000 mbar. Air flow rate was controlled by a mass flow meter (1559A Mass-Flo[®] Controller, MKS Instruments, Andover, Ma, USA [40]) covering the range from 20 to 200 slm (standard l/min).

Acquisition and control system was remote controlled by a personal computer using a LabVIEW dedicated software developed by the QEPM Research Group [4]. Acquisition hardware included an ethernet “CompactDAQ” chassis (NI cDAQ-9188XT, National Instruments Corporation, Austin, TX, USA) that allowed the introduction of eight input/output cards. Typical

Fig. 4 Functional scheme of “STARDUST-Upgrade” [4]



experiment procedures are summarized in the experiment flowchart shown in Fig. 5.

“STARDUST-Upgrade” set-up, border conditions, and procedures for the experiments performed are described in detail in the following sections.

Pressurization Experiments

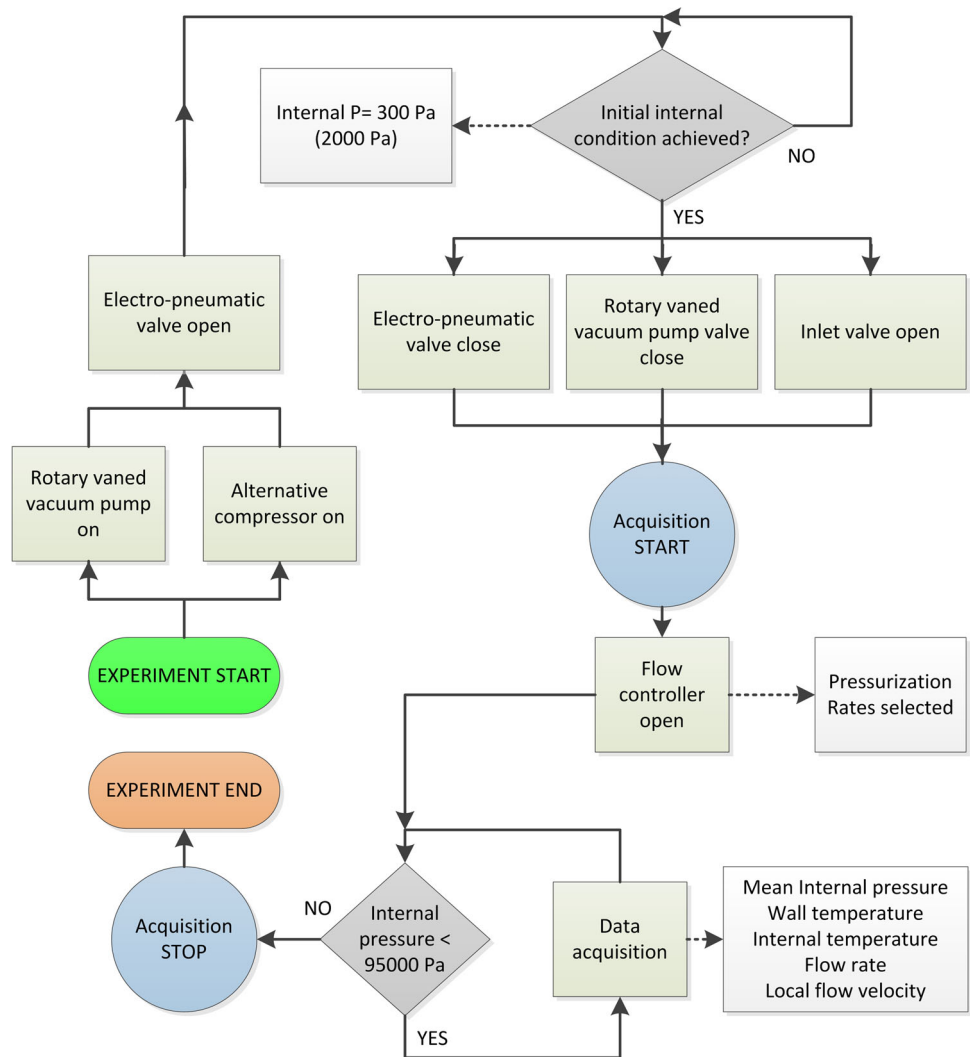
Materials and Methods

As a preliminary trial stage to demonstrate the capability of “STARDUST-Upgrade” to reproduce the thermo fluid-dynamic consequences expected in a LOVA accident, the facility was operated at different air inlet flow rates from different ports. In this set of experiments initial internal pressures chosen were 300 and 2000 Pa and final internal pressure was 95,000 Pa.

Ports used were C and D (see Figs. 2, 3), located in the upper part of the chamber. At least three replications were carried out for each of the eight experimental set-ups: 300-27-95-C, 300-27-95-D, 2000-27-95-C, 2000-27-95-D, 300-40-95-C, 300-40-95-D, 2000-40-95-C, 2000-40-95-D [where “XXXX-XX-XX-X” stands for “initial pressure (Pa)—flow rate (l/min)—final pressure (kPa)—port”].

Air flowed inside the chamber at a known mass flow rate from selected inlet port when the chamber reached target pressure (i.e. desired vacuum level). Boundary conditions were: initial internal pressure (Pa), final pressure (Pa), and volume flow rate (l/min), that were manually entered in LabVIEW dedicated software developed by the authors. Acquisition data sampled at 50 Hz during the entire intake process included: observation #, actual internal pressure (Pa), j-thermocouples temperatures T2 (°C), T3 (°C), T4 (°C), intake air volume flow rate (l/min). Data analysis with

Fig. 5 “STARDUST-Upgrade” typical experiment protocol flowchart [3]



Matlab script developed by the authors produced results presented in following section.

Results

Graphs shown below were produced for each replication showing trends for the following quantities during the whole air intake process after vacuum rupture: internal pressure (Pa); mean temperature (K) (calculated as arithmetic mean of the three j-thermocouples temperatures T2, T3, T4, see Fig. 4); air flow rate (l/min).

Average temperature and air flow rate graphs for all set-ups and replications presented similar trends to what shown in Fig. 6 and so are not all shown in this paper. In fact, the average internal temperature measured inside the chamber was room temperature for all replications (296.2 ± 2.2 K, Fig. 6). In addition, a graph for the flow rate for the first 6 s of the experiment is presented to appreciate the transient to reach target flow rate fixed. Target air flow rate was reached in about 2 s for all set-ups and replications, with a trend similar to that shown in Fig. 6.

Internal pressure trends (Fig. 7) are presented for 27 and 40 l/min air flow rate using two different initial internal pressure of the chamber (300 and 2000 Pa). Pressurization rates achieved (Pa/s) are reported. Direct error on Pirani pressure measure was $\pm 10 \div 15$ % [39].

Air Velocity Determination Experiments

Pressure transducers array have been positioned inside “STARDUST-Upgrade” facility at 0.5 cm from air inlet port C (Fig. 3) located in the upper part of the chamber to measure differential pressure of the air flow during pressurization experiments at different pressurization rates. Pressurization rates used for local air velocity calculation

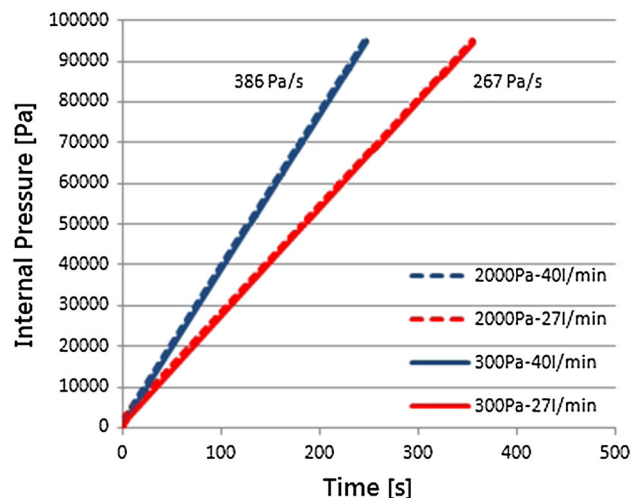


Fig. 7 Internal pressure trends measured by Pirani gauge inside “STARDUST-Upgrade” facility during air intake process due to vacuum failure

were 267 and 386 Pa/s (presented in Fig. 7) corresponding respectively to 27 and 40 l/min air flow rate. Hence the campaign was carried out using pressurization rate respectively lower and higher than the 300 Pa/s predicted in GSSR Report for ITER, with the objective to reproduce vacuum failure consequences comparable to those expected in ITER according to GSSR Report [35]. Air velocity experiments were carried out with two different initial internal pressure of the chamber (300 and 2000 Pa). Pressure transducers’ voltage output (mV) was acquired and converted into differential pressure (Pa) according to its sensitivity, and saved for further elaborations and error analysis. Objective of this experiment was to calculate air velocity according to air differential pressure measured by pressure transducers array and chamber temperature measured by thermocouples.

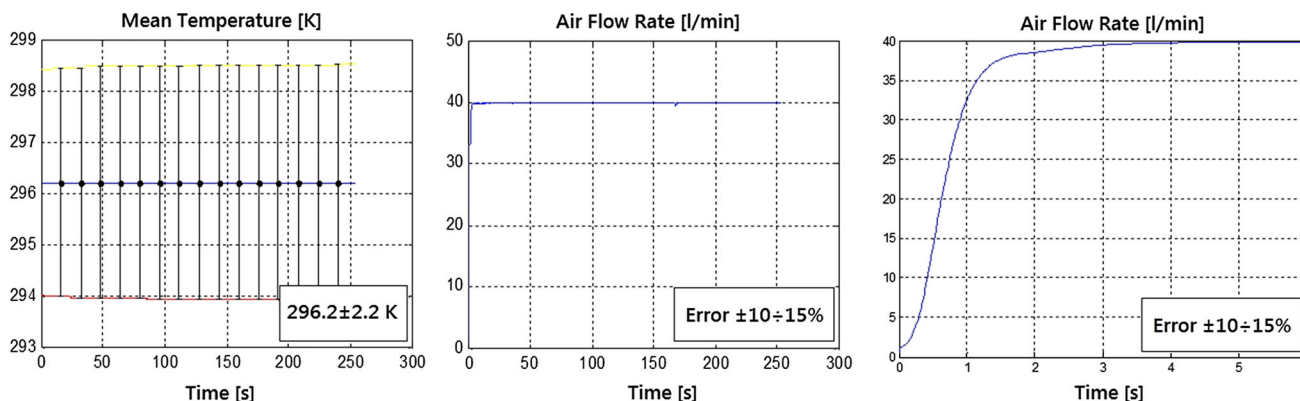


Fig. 6 Mean Temperature and Air Flow rate trend during pressurization at 40 l/min flow rate for inlet from port C starting from 2000 Pa (replication #3, 2000-40-95-C)

Materials and Methods

In this set of experiments initial internal pressure chosen was 2000 and 300 Pa and final internal pressure 95,000 Pa. Volume flow rate chosen was 27 and 40 l/min. Port used was port C (see Figs. 2, 3), located in the upper part of the chamber. Experiments were carried out with four experimental set-ups: 2000-27-95-C, 2000-40-95-C, 300-27-95-C, 300-40-95-C [where “XXXX-XX-95-C” stands for “initial pressure (Pa)—flow rate (l/min)—final pressure (kPa)—port used”].

Air flowed inside the chamber at a known mass flow rate from selected inlet port when the chamber reached target

$$v dv + g dz + dh = dq + dl \Rightarrow \int v dv + \int dh = 0 \Rightarrow \frac{v^2}{2} + (h - h_0) = 0 \Rightarrow v = \sqrt{2(h_0 - h)} \quad (1)$$

pressure. Boundary conditions were: initial internal pressure (Pa), final pressure (Pa), and volume flow rate (l/min), that were manually entered in LabVIEW software. Acquisition at 50 Hz during the entire intake process included data on: observation #, actual internal pressure (Pa), j-thermocouples temperatures T2 (°C), T3 (°C), T4 (°C), intake volume flow rate (l/min), Kulite pressure transducers voltage output signal (mV). Data analysis was carried out using both a Microsoft Excel2007 VBA script and a Matlab script developed by the authors. Graphs are presented for air velocity calculated according to Eq. (3) presented in “Air Velocity Calculation Model and Error Analysis” section, as a function of data saved throughout the experiments in terms of: internal pressure (Pa); mean temperature (K) (calculated as arithmetic mean of the three temperatures T2, T3 and T4); Kulite pressure transducer voltage output signal [mV].

The XCE-093-2D Kulite pressure transducers (XCE-093-2D High Temperature Miniature Pressure Transducer, Kulite Semiconductor Products, Inc., Leonia, NJ, USA [38]) are based on piezoresistive effect [39]. The pressure transducer gives a voltage output (up to 100 mV) that is converted into differential pressure according to its sensitivity. Differential pressure P_Δ is equal to the difference between dynamic pressure (measured by the sensor head) and the static pressure P_S (measured by the pressure reference tube). Noise of the pressure reference tube is reported to have a maximum value of ± 0.5 mV, so that is the offset (mV) acceptable for the transducer [38]. Operating temperature range is reported from -65 (-55 °C) to 525 °F (273 °C), and compensated temperature range from 25 to 235 °C [38]. However, experiments for this campaign are carried out at room temperature. Pressure transducer output (mV) was acquired in a NI 9219 card (24-bit

Universal Analog Input NI 9219, National Instruments Corporation, Austin, TX, USA) at 50 Hz and saved for further elaborations and error analysis [8].

All local air velocity graphs presented include error bars calculated according to error analysis described in following section.

Air Velocity Calculation Model and Error Analysis

According to the First Law of Thermodynamics for an open system, assuming steady state operations, altitude term negligible ($gdz = 0$), isentropic process (no heat transfer $dq = 0$), and no work done ($dl = 0$):

where v is air velocity (m/s) and h enthalpy (J/kg). Moreover, h_0 represents stagnation (or total) enthalpy, the enthalpy that the flow (of air in this case) would possess if brought to rest (zero velocity, $v_0 = 0$) isentropically from velocity v .

Considering compressible air as a perfect gas, its velocity can be determined as:

$$v = \sqrt{2c_p(T_0 - T)} = \sqrt{2c_p T \left(\frac{T_0}{T} - 1 \right)} \\ = \sqrt{\frac{2k}{k-1} \frac{RT}{M} \left[\left(\frac{p}{p_0} \right)^{\frac{k-1}{k}} - 1 \right]} \quad (2)$$

where:

- $k = c_p/c_v$, Ratio of the fluid specific heat at constant pressure c_p to the fluid specific heat at constant volume c_v (it is approximately equal to 1.4 for air at standard condition);
- $R = 8.314 \text{ JK}^{-1} \text{ mol}^{-1}$ Universal gas constant;
- $M = 0.028968 \text{ kg/mol}$ Dry air molecular mass at standard conditions.

Since temperature T refers to mean temperature \bar{T} of the chamber measured with i thermocouples as $\bar{T} = \frac{1}{N} \sum_{i=1}^N T_i$, and pressure p refers to total pressure P_T (measured by Kulite pressure trasducer head), and since “zero” pressure (p_0) refers to static pressure P_S (measured by trasducer pressure reference tube), and knowing that $P_\Delta = P_T - P_S$, the previous equation can be re-written as:

$$v = \sqrt{\frac{2k}{k-1} \frac{R\bar{T}}{M} \left[\left(\frac{P_\Delta}{P_S} + 1 \right)^{\frac{k-1}{k}} - 1 \right]} \quad (3)$$

where:

- $\bar{T} = \frac{1}{N} \sum_{i=1}^N T_i$ Mean temperature from i thermocouples (K);
- P_S Static pressure (measured by Pirani pressure gauge);
- $P_\Delta = P_T - P_S$ Differential pressure (measured by pressure transducers as difference between head pressure and reference tube pressure);
- P_T Total pressure (measured by transducers head).

Experimental measurements are affected by both hardware direct errors and propagation of uncertainty in case of indirect measurements, like in this case velocity.

Velocity function $v = f(x_1, x_2, x_3)$ depends on: $x_1 = \bar{T}$ (mean temperature from J-thermocouples), $x_2 = P_S$ (static pressure from Pirani pressure gauge), $x_3 = P_\Delta$ (differential pressure from Kulite pressure transducers). If all the three uncertainties $\Delta x_1, \Delta x_2, \Delta x_3$ on the variables are not likely to have the same sign, and if correlations among variables x_1, x_2, x_3 are neglected hence assuming that variables are independent, it is possible to use the following Eq. (6) [41] for total uncertainty Δv of velocity:

$$\Delta v = \sqrt{\left[\left(\frac{\partial f}{\partial x_1} \right) \Delta x_1 \right]^2 + \left[\left(\frac{\partial f}{\partial x_2} \right) \Delta x_2 \right]^2 + \left[\left(\frac{\partial f}{\partial x_3} \right) \Delta x_3 \right]^2} \tag{4}$$

where:

$$\frac{\partial f}{\partial x_1} = v'(\bar{T}) = \frac{1}{2\bar{T}} \sqrt{\frac{2k}{k-1} \frac{R\bar{T}}{M} \left[\left(\frac{P_\Delta}{P_S} + 1 \right)^{\frac{k-1}{k}} - 1 \right]} \tag{5}$$

$$\frac{\partial f}{\partial x_2} = v'(P_S) = \frac{P_\Delta R \bar{T} \left(\frac{P_\Delta}{P_S} + 1 \right)^{\frac{k-1}{k}}}{MP_S^2 \sqrt{\frac{2k}{k-1} \frac{R\bar{T}}{M} \left[\left(\frac{P_\Delta}{P_S} + 1 \right)^{\frac{k-1}{k}} - 1 \right]}} \tag{6}$$

$$\frac{\partial f}{\partial x_3} = v'(P_\Delta) = \frac{R\bar{T} \left(\frac{P_\Delta}{P_S} \right)^{-\frac{1}{k}}}{MP_S \sqrt{\frac{2k}{k-1} \frac{R\bar{T}}{M} \left[\left(\frac{P_\Delta}{P_S} \right)^{\frac{k-1}{k}} - 1 \right]}} \tag{7}$$

Uncertainties $\Delta x_1, \Delta x_2, \Delta x_3$, (direct errors) on the three variables \bar{T}, P_S, P_Δ are [8]:

$$\Delta x_1 = 0.0031 \cdot \bar{T}(t)$$

$$\Delta x_{2, \text{PIRANI}} = 0.1 \cdot P_S(t) \text{ (pressure from 0.0005 to 1000 mbar)}$$

$$\Delta x_{2, \text{EDWARD}} = 0.002 \cdot P_S(t) \text{ (pressure from 1000 to 2000 mbar)}$$

$$\Delta x_3 = 0.1 \cdot P_\Delta(t)$$

where $\bar{T}(t), P_S(t)$ and $P_\Delta(t)$ are functions of time acquired throughout the experiments.

Velocity Transient Time Calculation

According to specifications presented in “Materials and Methods” section. Kulite transducers present a maximum acceptable offset corresponding to 0.5 mV. In other terms, every signal $-0.5 \text{ mV} < V^* < +0.5 \text{ mV}$ is considered not reliable. Air velocity [according to Eq. (3)] for a signal of 0.50 mV from Kulite transducer was calculated and reported in Table 2 [i.e. “v(0.50 mV)”. Every air velocity value smaller than that calculated for 0.50 mV is not considered in the analysis.

The “velocity transient time” (Table 2) was calculated as the interval from the start of air intake process to the time at which the pressure transducer voltage signal decreased till 0.50 mV, corresponding to its maximum acceptable zero point [38], and so corresponding to the minimum velocity calculated by the system above signal-to-noise ratio (SNR) (see Fig. 8). This velocity, namely “v(0.50 mV)”, is equal to the minimum air velocity detectable by the system. In the present work, “velocity transient time” was defined for all replications in order to have information on time range in which mobilization is expected, at different pressurization rates.

Results and Comparison with Numerical Model

Results are presented for four experimental set-ups: 2000-27-95-C, 2000-40-95-C, 300-27-95-C, 300-40-95-C [where “XXXX-XX-95-C” stands for “initial pressure (Pa)—flow rate (l/min)—final pressure (kPa)—port used”].

Graphs are presented for air velocity calculated according to Eq. (3), according to data saved throughout the experiments in terms of: internal pressure (Pa); mean temperature (K) (calculated as arithmetic mean of the three temperatures T2, T3 and T4). Graphs include error bars calculated according to error analysis described in “Air Velocity Calculation Model and Error Analysis” section.

Air velocity trends for first 25 s of air intake are reported in Fig. 9 that shows a velocity peak in the first 4 s. The corresponding pressurization rates are that shown in Fig. 7.

Table 2 summarizes results on air velocity calculations. The maximum velocity value (m/s) is presented for each run along with corresponding time (s) at which the maximum was observed. Velocity transient time (s) and corresponding velocity “v(0.50 mV)” are also reported.

Table 2 Air velocity calculation data sheet for 27 l/min and 40 l/min air flow rate at two different initial internal pressures (300 Pa and 2000 Pa) of the chamber of “STARDUST-Upgrade” facility

| | Flow rate [l/min] | | | | | |
|---------------------------------|-------------------|--------|--------|--------|--------|--------|
| | 40 | | | 27 | | |
| | Replication | | | | | |
| | #1 | #2 | #3 | #1 | #2 | #3 |
| <i>Initial pressure 300 Pa</i> | | | | | | |
| Max velocity [m/s] | 481.88 | 479.92 | 480.87 | 457.69 | 459.71 | 458.55 |
| Time [s] | 3.36 | 3.36 | 3.36 | 2.80 | 2.80 | 2.80 |
| Velocity transient time [s] | 58.69 | 57.78 | 55.56 | 45.97 | 49.17 | 48.20 |
| v(0.50 mV) | 48.32 | 37.68 | 40.23 | 56.35 | 49.12 | 45.93 |
| <i>Initial pressure 2000 Pa</i> | | | | | | |
| Max velocity [m/s] | 377.91 | 407.19 | 375.34 | 339.93 | 334.84 | 342.45 |
| Time [s] | 1.40 | 1.40 | 1.40 | 1.40 | 1.40 | 1.40 |
| Velocity transient time [s] | 44.54 | 66.53 | 44.06 | 52.50 | 51.36 | 54.55 |
| v(0.50 mV) | 40.03 | 30.52 | 40.18 | 42.92 | 49.67 | 42.84 |

Fig. 8 Kulite pressure transducer voltage signal graph showing velocity transient time (44.54 s) for run 2000-40-95-C-1. Equation on the right corresponds to the black trendline

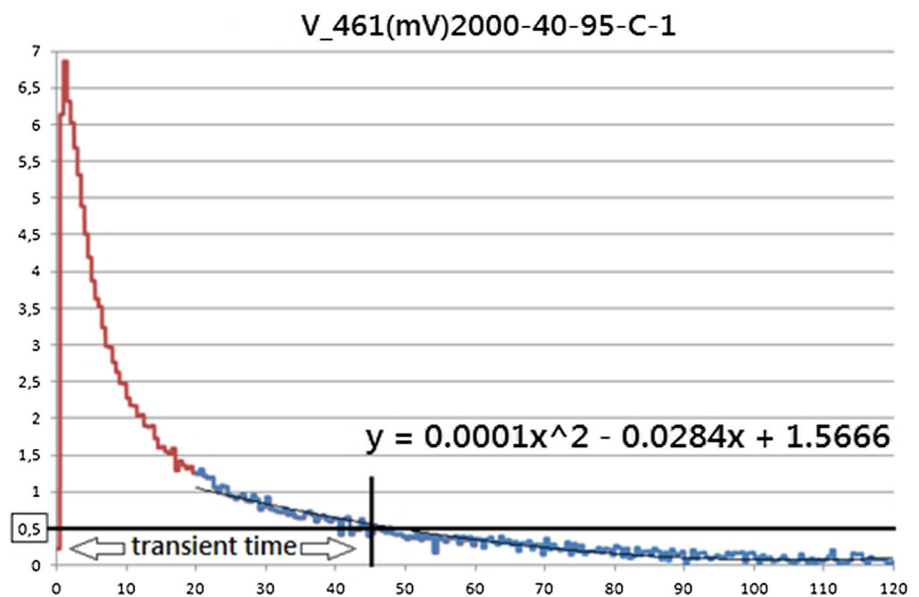


Table 2 summarize results for all replications for different flow rates (27 and 40 l/min) and different initial internal pressure of the chamber (300 and 2000 Pa).

Figure 10 compares “2000-27-95-C” pressurization curve measured experimentally (and presented with error bars due to Pirani gauge direct error) with CFD model prediction. Figure 11 presents numerical and experimental air velocity trends for air intake at 27 l/min. Experimental and numerical results show substantial agreement for the first 20 s of pressurization, that are crucial for resuspension phenomena investigation as evidenced by velocity transient time data presented in Table 2. However, due to numerical viscosity effects, the numerical velocity predicted peak in

the first seconds is lower than the experimental one (Fig. 11).

Conclusions

Pressurization of the chamber achieved through air intake from upper ports C and D (Figs. 2, 3) evidenced that “STARDUST-Upgrade” facility is able to reproduce a wide range of pressurization rates including what expected in GSSR Report [35], not only from the lower and equatorial level [1–8, 17] but also from the upper section of the vessel. Experiments carried out with 40 and 27 l/min air

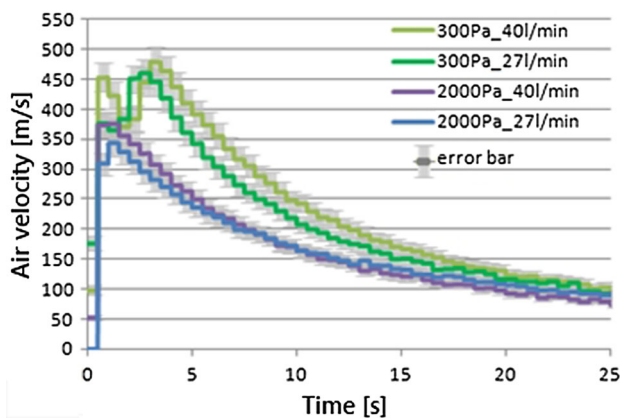


Fig. 9 Air velocity trends calculated for pressurization experiments in “STARDUST-Upgrade” facility

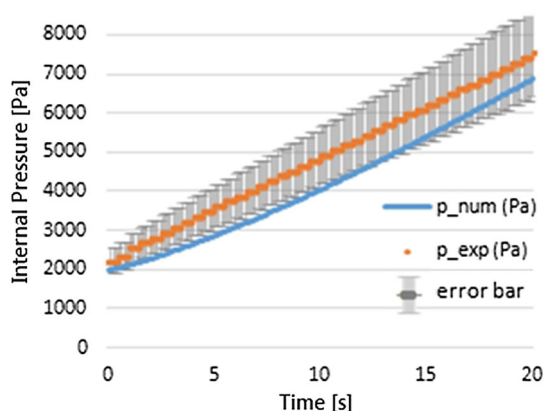


Fig. 10 Measured internal pressure of the chamber with error bars (p_{exp}) compared to model prediction (p_{num}) for air intake at 27 l/min at 2000 Pa initial internal pressure

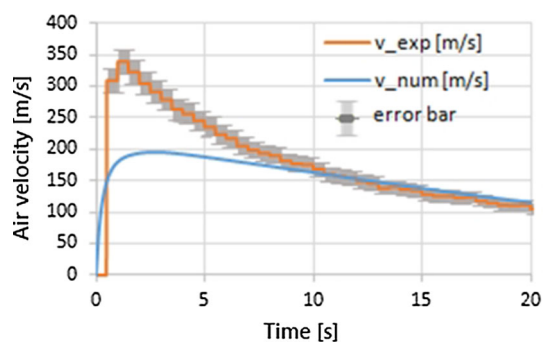


Fig. 11 Measured air velocity at the outlet of port C (v_{exp}) compared to model prediction (v_{num}) for air intake at 27 l/min at 2000 Pa initial internal pressure

intake presented a pressurization rate respectively of 386 and 267 Pa/s (Fig. 7). Chamber reached final pressure in about 1000 s in all replications. Flow rate transient in the first seconds evidenced that target flow rate fixed by the

mass flow meter is achieved in about 2–3 s. This is due to the delay on the inlet feed valve opening after signal is received from the control system. This valve needs an input of 220 V given by an external relay controlled by the software. Temperatures measured by j-thermocouples placed inside the vacuum chamber presented same trend for all experiments. Experiment were carried out at room temperature and no heating source was used hence temperatures presented a flat trend throughout the experiment: mean temperature was considered constant (Fig. 6).

As expected, all air velocity trends (Fig. 9) were similar and presented a sudden rise in the first seconds leading to the maximum air velocity value summarized in Table 2. The maximum air velocity value increased with flow rate for both initial pressures chosen. Velocity peak increased of about 20 and 50 m/s (respectively for initial internal pressure equal to 300 and 2000 Pa) when flow rate increased from 27 to 40 l/min.

The Transient velocity time shown in Table 2 resulted smaller than 60 s for all replications demonstrating that investigation of dust mobilization is crucial in the first seconds.

In some replications (e.g. “300Pa_40 l/min”, Fig. 9) air velocity trend presented another peak just before the expected one. This unexpected peak was assumed to be the result of a shock wave caused by the vacuum breach. Unfortunately, the acquisition frequency used (50 Hz) was not enough to investigate the shock wave phenomenon. Higher resolution is needed.

Furthermore, Figs. 10, 11 show a substantial agreement between numerical and experimental results in terms of pressurization of the chamber and local air velocity. It is observed that the simulated air velocity trend does not reach the same measured peak value, and that the predicted pressurization rate is lower than the experimental one. This could be due to an insufficiently fine grid, which produces numerical viscosity. Future model development should improve the numerical accuracy. As a next step for this research, the discrepancy between velocity measurements and CFD calculations in the first 10 s must be investigated in detail and completely understood.

As a first step to demonstrate the capability of “STARDUST-Upgrade” facility to reproduce LOVA conditions comparable to those expected in ITER, this work presented the preparatory procedures for the fine tuning of the facility. We demonstrated that the facility is capable of reproducing some of the thermo fluid-dynamic consequences of a LOVA from lower, equatorial and upper part of an ITER-like vacuum vessel, in terms of expected pressurization rates and local air velocity. Results are presented for two different pressurization rates. Since the fluid expected to enter the vessel during a LOCA could be different from air, next experimental campaign will involve

different fluid (e.g. steam) to also reproduce a LOCA event. We believe this work is an important starting point and will be continued with the final goal of completely reproduce, characterize, and simulate the dust mobilization phenomena in case of vacuum rupture of the vacuum vessel of nuclear fusion reactors.

Conflict of interest The authors declare that they have no conflict of interest.

References

- J.P. Sharpe et al., *Fusion Eng. Des.* **63–64**, 153–163 (2002)
- J. Winter, *Phys. Plasmas* **7**, 3862–3866 (2000)
- A. Malizia et al., *Adv. Mat. Sci. Eng.* **2014**, Article ID 201831, 29 (2014)
- A. Malizia, in *35th EPS Conference on Plasma Physics* **32**, 696–699 (2008)
- C. Bellecci et al., *Fusion Eng. Des.* **86(9–11)**, 2774–2778 (2011)
- D. Di Giovanni et al., *WSEAS Trans. Environ. Dev.* **10**, 106–122 (2014)
- A. Malizia et al., in *41st EPS Conference on Plasma Physics*, (2014), p. 5006
- A. Malizia, *Radioactive dust re-suspension/mobilization inside tokamaks* (LAP LAMBERT Academic Publishing, Saarbrücken, 2014)
- K. Takase et al., *Fusion Eng. Des.* **42**, 83–88 (1998)
- A. Malizia et al., *Def. S T Tech. Bull.* **4(1)**, 64–76 (2011)
- A. Malizia et al., *Def. S T Tech. Bull.* **5(1)**, 36–45 (2012)
- O. Cenciarelli et al., *Def. S T Tech. Bull.* **6(1)**, 33–41 (2013)
- J.P. Sharpe, P.W. Humrickhouse, *Fusion Eng. Des.* **81**, 1409–1415 (2006)
- W.G. Brown, *Int. J. Heat Mass Transf.* **5**, 859–871 (1962)
- K. Takase et al., *Fusion Tech.* **30**, 1459–1464 (1996)
- K. Takase et al., *Nucl. Sci. Eng.* **125**, 223–231 (1997)
- I. Lupelli et al., *J. Fusion Energ.* ISSN 0164-0313 (2015). doi:10.1007/s10894-015-9905-8
- K. Takase, *Fusion Eng. Des.* **54**, 605–615 (2001)
- P. Gaudio et al., in *International Conference on Mathematical Models for Engineering Science*, (2010), pp. 134–147
- P. Gaudio et al., *Int. J. Syst. Appl. Eng. Dev.* **5**, 287–305 (2011)
- M. Benedetti et al., *Int. J. Syst. Appl. Eng. Dev.* **5**, 718–727 (2011)
- M. Benedetti et al., *Fusion Eng. Des.* **88(9–10)**, 2665–2668 (2013)
- C. Bellecci et al., *Fusion Eng. Des.* **88(9–11)**, 2774–2778 (2011)
- C. Bellecci et al., *Nucl. Fusion* **51(5)**, 053017 (2011)
- C. Bellecci et al., *Fusion Eng. Des.* **86(4–5)**, 330–340 (2011)
- M. Benedetti et al., in *Mechanics RRI*, ed. 2nd International Conference on FLUIDSHEAT'11, TAM'11. 4th WSEAS International Conference on UPT'11, CUHT'11, (2011), pp. 142–147
- T. Pinna et al., *Fusion Eng. Des.* **85(7–9)**, 1410–1415 (2010)
- C. Bellecci et al., in *37th EPS Conference on Plasma Physics*, (2010), pp. 703–706
- P. Gaudio et al., in *International Conference on Mathematical Models for Engineering Science (MMES' 10)*, (2010), pp. 134–147
- C. Bellecci et al., in *33E1 ECA*, ed. *36th EPS Conference on Plasma Physics*, (2009), pp. 266–269
- C. Bellecci et al., in *32 EP*, ed. *35th EPS Conference on Plasma Physics*, vol. 32 (2008), pp. 9–13
- I. Lupelli et al., *Fusion Eng. Des.* **89(9–10)**, 2048–2052 (2014)
- A. Malizia et al., *Fusion Eng. Des.* **89(9–10)**, 2098–2102 (2014)
- P. Gaudio et al., *ICFDT 2013 Conference* (INFN, Frascati, 2013)
- IAEA. ITER Joint Central Team. *Generic Site Safety Report (GSSR)*. https://fusion.gat.com/iter/iter-fdr/final-report-sep-2001/Plant_Assembly_Documents_%28PADs%29/Generic_Site_Safety_Report_GSSR/GSSR_09_ExtHazAssmnt.pdf, Accessed: 11 Dec 2014
- A. Malizia et al., *Fusion Eng. Des.* Available online 19 December 2014. In Press. doi:10.1016/j.fusengdes.2014.11.009
- Kulite Semiconductor Products, Inc., Leonia, Nj, USA. www.kulite.com/docs/products/XCE-093.pdf, Accessed: 11 Dec 2014
- A. Kurtz, J. VanDWeert, B. Kochman, *Pitot-static Transducer*, Kulite Semiconductor Products, Inc., Leonia, Nj, USA
- Alcatel Vacuum Technology, Annecy, France. *Alcatel AP 1004 Pirani Gauge Specifications*. www.pfeiffer-vacuum.com/downloads/container.action, Accessed: 11 Dec 2014
- MKS Instruments, Andover, Ma, USA. *General Purpose Mass-Flow(R) Controller 1559A* www.mksinst.com/docs/ur/1559.pdf, Accessed: 4 Feb 2015
- H.H. Ku. *J. Res. Natl. Bur. Stand C Eng. Instrum.* **70C(4)**, (1966)